THE JOURNAL OF PHYSICAL CHEMISTRY B LETTERS

2005, *109,* 17361−17365
Published on Web 08/27/2005

Field-Effect Characteristics and Screening in Double-Walled Carbon Nanotube Field-Effect Transistors

S. Wang,[†] X. L. Liang,[†] Q. Chen,*[,†] Z. Y. Zhang,[‡] and L.-M. Peng*[,†,‡]

Key Laboratory for the Physics and Chemistry of Nanodevices and Department of Electronics, Peking University, Beijing 100871, and Institute of Physics, Chinese Academy of Sciences, Beijing 100080, China

Received: July 8, 2005; In Final Form: August 12, 2005

Field-effect transistors (FETs) have been fabricated using double-walled carbon nanotubes (DWCNTs), and electrical transport measurements have been carried out on 125 DWCNT FETs. Among these devices, 52 were found to show basically semiconducting field-effect characteristics, 44 show metallic characteristics, and 29 show neither pure semiconducting nor metallic characteristics. These 3 distinct types of field-effect characteristics were identified as resulting from the semiconducting (S)−S, metallic (M)−M or M−S, and S−M combinations of the two shells of the DWCNT. While the S−S and M−M or M−S DWCNT devices exhibit similar field-effect characteristics to those by single-walled carbon nanotube (SWCNT) devices, the S−M device responds uniquely to the external gate voltage. In particular, it was found that free charges in the inner metallic shell may screen the outer semiconducting shell from the gate effect and that the screening is directly related to the intershell interaction, which increases with increasing temperature and tube diameter. The screening is disadvantageous to the performance of DWCNT FETs, and a similar effect is expected to occur in MWCNTs.

Introduction

The electronic properties of carbon nanotubes (CNT) have been extensively studied throughout the past decade.[1−6] However, there remain several outstanding problems concerning the electronic transport of multiwalled carbon nanotubes (MWCNTs) due to their complicated structures and intershell interactions. In this regard, a double-walled carbon nanotube (DWCNT), being the simplest MWCNT, presents a perfect testing system for investigating the effects of intershell interactions on the transport properties of MWCNTs.

The characteristics of intershell interactions of MWCNTs have been studied theoretically.[7−10] It was predicted that intershell interactions may block some quantum conductance channels and lead to integer and noninteger quantum conductance,[7] the electron wave packet can spread over several shells,[8] the separation of degenerated energy levels due to intershell interactions can lead to reduction of conductance,[9] and charges can transfer between neighboring shells resulting in interlayer states.[10] However, only a few experiments have been reported concerning with the electrical transport in DWCNTs.[11,12] The field-effect transistors (FETs) based on DWCNTs were found to exhibit either ambipolar or metallic behavior.[12] In previous reports on MWCNTs,[13−16] the electric properties of a MWCNT were characterized mainly by the outmost shell of the tube at low bias or low temperature, but finite contribution from inner shells of a MWCNT was also noticed. While some studies concluded that the intershell transfer of carriers results largely from thermal activation and the contribution from the inner shell depends both on the temperature and the bias,[14,15] it was proposed[16] that the intershell conductance is via orbital coupling that hardly depends on temperature. In this work, FETs have been fabricated using DWCNTs, and their electrical transport characteristics been investigated.

Experimental Section

The DWCNTs used in this study were synthesized by catalytic decomposition of methane at 1373 K.[17] Shown in Figure 1a,b are transmission electron microscopy (TEM) images of two DWCNTs having a diameter of 2.5 nm and 4.9 nm, respectively. These DWCNTs were dispersed by sonication in dichloroethane and dropped onto a Si substrate. The Si substrate was heavily doped and covered by either a 200-nm or 20-nm-thick thermally grown SiO_2 layer and was used as the back gate for field-effect measurements. The Pd electrodes of 20 nm thickness were defined by electron-beam lithography on individual DWCNTs. The total resistance of the device in the "on" state (hole transport) ranges from 20 kΩ to 300 kΩ, and for devices showing strong field effect, the resistance can be increased by several orders of magnitude by switching from the on state to the off state via increasing gate voltage. Low-temperature electrical measurements were carried out using a Janis cold stage and a semiconductor characterization system KEITHLEY 4200. The diameters of the DWCNTs were estimated using both transmission electron microscopy (TEM) and atomic force microscope (AFM) (Digital Instruments DI3100/ Nano Scope IV).

* To whom correspondence should be addressed. E-mail addresses: qingchen@pku.edu.cn (Q.C.) and lmpeng@pku.edu.cn (L.M.P.).
[†] Peking University.
[‡] Chinese Academy of Sciences.

10.1021/jp053739+ CCC: $30.25

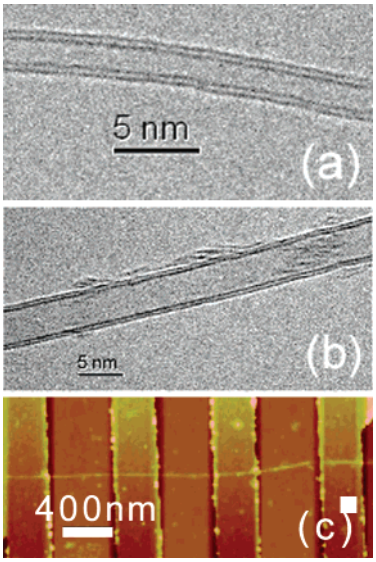

Figure 1. TEM images showing a single DWCNT with a diameter of (a) 2.5 nm and (b) 4.9 nm. In (c) is an AFM image showing a typical DWCNT FET. The width of the Pd electrode is about 400−500 nm, and the DWCNT channel length between the electrodes is about 500−600 nm.

Results and Discussions

In this investigation, more than 200 DWCNT devices were fabricated. Among these devices, 125 were found to function well and were therefore carefully measured. It should be noted that the structure of the DWCNT was not precisely controllable. The measured 125 devices were therefore not identical and may differ in tube diameter, channel length, helical angle, and so forth, and the large sampling provides us with an opportunity to investigate the dependence of the device on such parameters as tube diameter and the nature of the two shells of the DWCNT. For a DWCNT, we may have four distinct shell−shell combinations, i.e., metallic (M)-semiconducting (S), M−M, S−M, and S−S, and the three types of distinct field-effect characteristics were identified to correspond respectively to the (1) S−S, (2) S−M, and (3) M−M or M−S combinations. Among the 125 tested devices, we found 52 devices exhibiting S−S characteristics (see Figure 2), 29 devices exhibit S−M characteristics (see Figure 3a), and 44 devices exhibit M−S or M−M characteristics (see Figure 3b). These three distinct types of field-effect characteristics can be easily identified. For the S−S device (Figure 2), the current may be most effectively changed by changing the gate voltage, an "off" state may always be identified as having nearly zero current, and the I_{on}/I_{off} ratio is larger than 10^2. For the S−M device (Figure 3a), the I_{on}/I_{off} ratio is typically less than 10, the transition region from "on" state to "off" state is much wider than that for the S−S device, and once reduced from the "on" state in the hole transport region (with large negative V_g), the current hardly shows any recovery in switching into the electron transport region (with large positive V_g). For the M−M or M−S device (Figure 3b), the current hardly shows any significant variation with gate voltage. Assuming that the structures of the two shells of the DWCNT are totally uncorrelated, we would expect about $^4/_9$ of the devices be of the S−S type, i.e., 55, $^2/_9$ of the devices or 28 be of the S−M type, and $^3/_9$ of the devices or 42 be of the M−S and M−M type. Our experimental results (S−S, 52; S−M, 29; M−M or M−S, 44) are indeed very close to this simple prediction, confirming not only our classifications of the field-effect characteristics but also that there exists very little correlation between the nature of the two shells of the DWCNT.

Shown in Figure 2 are room-temperature source-drain current (I_{ds}) vs gate voltage (V_g) curves of two DWCNT FETs. The source-drain current I_{ds} was measured as a function of the gate voltage V_g, and the two curves shown in Figure 2a,b were measured respectively for a DWCNT with a diameter of 3.0 nm and 4.5 nm. Both DWCNT FETs show a hole transport region for $V_g < -15$ V, and the hole transport switched to electron transport for $V_g > -4$ V. The on/off ratio I_{on}/I_{off} is about 10^4 for the smaller DWCNT (Figure 2a), and this ratio reduces to about 10^2 for the larger DWCNT (with smaller band gap) of Figure 2b. In both cases, the current at the off state between $V_g = [-11\text{ V}, -7\text{ V}]$ became less than 7×10^{-10}A. This shows that the current in the conducting DWCNT channel was almost completely depleted of carriers, suggesting that the two shells of the DWCNTs are both of the semiconducting type. The on-state current in the hole transport region is much larger than that in the electron transport region, and this behavior is very different from the ambipolar behavior reported in ref 12. The discrepancy results from the fact that in ref 12 Ti/Au contacts were used, while in this work, Pd was used. The Fermi level of the former electrodes was known to lie near the middle of the band gap of the carbon nanotube, while the Pd contact was known to favor hole transport.[6] The relative current level in the electron transport region is seen to be larger for the larger DWCNT of Figure 2b than that for the smaller DWCNT of Figure 2a, and this difference may be attributed to the band gap dependence of the CNT on its diameter d, i.e., $E_g \approx 0.8$ eV/d, since smaller E_g results in less band bending[18] at the electron transport region and therefore better electron conductance and larger current.

In addition to the S−S behavior shown in Figure 2, two more distinct types of field-effect characteristics are shown in Figure 3. Figure 3a was obtained from a DWCNT of 2.4 nm showing an apparent on-state for hole transport at $V_g < -5$ V and finite current at all other gate voltages, and no true off-state was observed. The fact that this DWCNT shows strong field effect at the hole transport region suggests that the conductance is mainly semiconducting in nature, while the observation that the conducting channel cannot be turned off completely at all gate voltage suggests that the metallic conductance channel was also involved. We therefore conclude that the DWCNT of Figure 3a is of the S−M type. Unlike Figures 2 and 3a, Figure 3b shows that the current hardly depends on the gate voltage. This is typical metallic behavior,[14,15] and the DWCNT involved could be either M−M type or M−S type. In both cases, the conductance is dominated by the outer metallic shell of the DWCNT.

While the S−S (Figure 2) and M−M or M−S (Figure 3b) types of field-effect characteristics bear analogy to that of a semiconducting or metallic single-walled carbon nanotube (SWCNT), the S−M type field-effect characteristics as shown in Figure 3a is unique of DWCNT in at least two aspects. First, while the DWCNT FET shows large conductance at the hole transportation region (with $V_g < -10$ V) at all temperatures, the current cannot be completely turned off at all gate voltages, and at room temperature, the on/off ratio I_{on}/I_{off} is typically less than 10, a ratio far lower than that can be achieved by S−S DWCNT FETs and SWCNT FETs of similar diameters (better than 10^2). Second, it was found that, for the S−M DWCNT FET, the current remains at basically the same level once the conductance was changed from the hole transport region ($V_g <$ 10 V) to the electron transport region ($V_g >$ 10 V). The transition region from the good hole-conduction region to the poor electron-conduction region was found to be much wider than

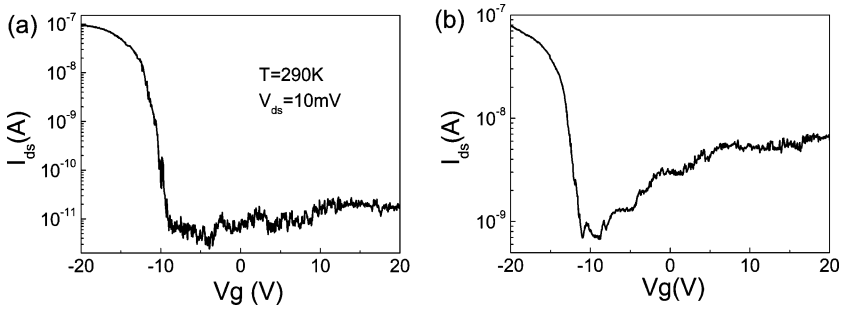

Figure 2. Source-drain current vs gate voltage for a DWCNT having (a) a diameter of 3 nm and length of 500 nm; (b) a diameter of 4.5 nm and length of 800 nm. The measurements were made at 290 K with a bias voltage of 10 mV.

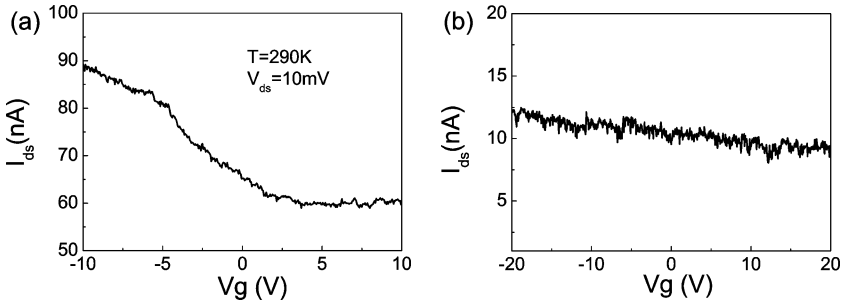

Figure 3. $I-V$ measurements for (a) a DWCNT with 2.4 nm diameter and $L = 1$ μm, and (b) a DWCNT with 4.5 nm diameter and $L = 0.8$ μm.

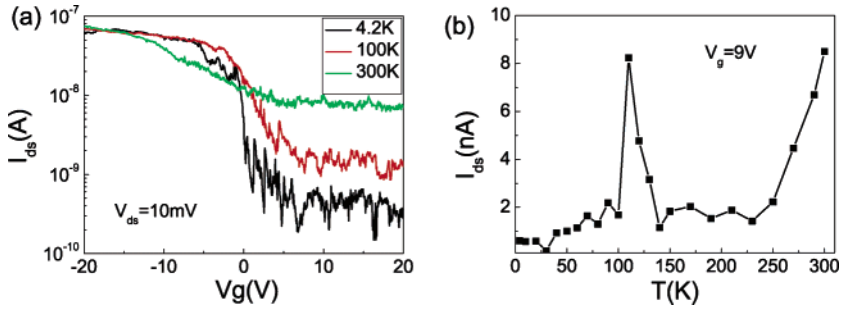

Figure 4. Temperature dependence of the source-drain current for a DWCNT FET (a) as a function of the gate voltage and (b) at a fixed gate voltage $V_g = 9$ V. The DWCNT has a diameter of 3 nm and a length of $L = 400$ nm.

that for a SWCNT FET. Figures 3a and 4a show that at room temperature this transition occurs at least over 10 V, and this transition region is at least several times wider than that of a SWCNT FET or a S−S DWCNT FET (see, e.g., Figure 2a). At lower temperature, the transition region becomes narrower, and the I_{on}/I_{off} ratio becomes larger (Figure 4a).

The total source-drain current of an S−M DWCNT FET may be written as a simple summation of the current passing through the outer semiconducting shell I_s and the inner metallic shell I_m

$$I_{ds} = I_s + I_m \tag{1}$$

and the current in the inner metallic shell reflects charge injection from the outer semiconducting shell and the intershell interaction. In the hole transport region, holes may be readily injected from the contact into the outer semiconducting shell, and the total current is dominated by I_s. As the gate voltage increases, the valence band of the outer semiconducting shell of the DWCNT is pulling down by the positive gate voltage and would eventually become nonconducting if the top of the valence band could be moved down below the Fermi level of the contact. As V_g increases, the outer semiconducting shell becomes less conductive. The free charges that have been transferred into the inner metallic shell become more influential. On one hand, the relative contribution of I_m to the total current increases with increasing V_g. On the other hand, the free charges on the inner metallic shell may rearrange themselves to reduce the effect of the gate voltage on the conducting DWCNT, i.e., charges in the metallic shell may screen the semiconducting shell from the influence of the gate to certain extend. As a result, the "hole-conduction" channel associated with the valence band of the outer semiconducting shell cannot be completely "turned off" even at a large positive V_g, and for the same reason, the "electron-conduction" channel associated with the conduction band of the semiconducting shell cannot be "turned on" using a gate voltage that is as large as 20 V.

The effectiveness of the screening of the inner metallic shell of the S−M DWCNT is determined by the intershell charge transfer or interaction. The residual current level at large positive V_g is determined by the balance between the gate effect and the screening, and the latter is determined by the amount of charges that have been transferred from the outer semiconducting shell into the inner metallic shell. The residual current level at large positive V_g therefore reflects directly the strength of the intershell interaction. Shown in Figure 4b is the temperature dependence of the residual current at $V_g = 9$ V. It is clear that the residual current tends to increase with increasing temperature (see also Figure 5b), and the general trend is superimposed by some fluctuating peaks and dips; these features are of random nature and may be attributed to, among other things, random

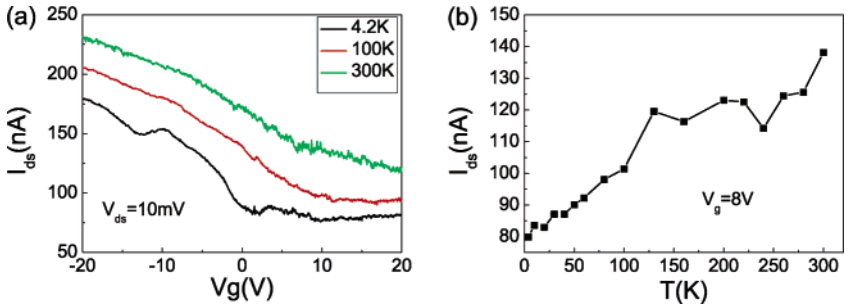

Figure 5. Source-drain current (a) as a function of gate voltage V_g for three temperatures and (b) as a function of temperature at a fixed gate voltage $V_g = 8$ V for a DWCNT with a diameter of 4 nm and a length of 400 nm.

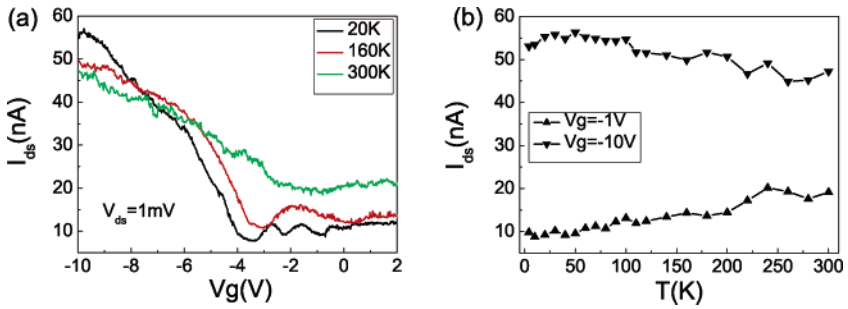

Figure 6. Source-drain current (a) as a function of gate voltage V_g for three temperatures and (b) as a function of temperature at two gate voltages $V_g = -10$ V and $V_g = -1$ V for a DWCNT with a diameter of 4 nm and a length of 300 nm. The thickness of the SiO_2 insulator layer is 20 nm.

adsorption and desorption processes on the outer surface of the semiconducting shell of the DWCNT.

The residual current level as shown in Figures 4b and 5b is determined mainly by charge transfer between the shells or the intershell coupling. In the hole transport region, the outer semiconducting shell of the DWCNT is wide open for hole conductance, and contribution from the inner metallic shell is only secondary. Toward the electron transport region, the resistance of the outer semiconducting shell becomes large, and more free charges are transferred into the inner metallic shell, and this not only contributes more to the current I_m but also affects the effectiveness of the gate via screening, making the field effect diminish. Figure 4a shows that at lower temperature the intershell coupling is weaker, and fewer carriers have been transferred into the inner metallic shell. As a result, the screening effect is weaker and gating is more effective, leading to a larger I_{on}/I_{off} ratio at lower temperature than at higher temperature. As temperature increases, the intershell interaction becomes stronger, and carriers may then be transferred into the inner metallic shell more effectively. The increased free charges in the metallic shell will tend to screen the effect of the gate, to pin down the energy bands of the semiconducting shell. The hole-conduction channel cannot therefore be "turned off" completely, and the electron-conduction channel cannot be "turned on" even at large positive gate voltage. The intershell coupling may be affected not only by temperature but also by certain random processes, such as adsorption and desorption on the outer surface of the semiconducting shell, and perhaps also by the presence of atoms between the shells. These effects affect the intershell coupling and add random current peaks and dips to Figures 4b and 5b. These features are not always present in the temperature-dependent curve of the residual current, but the current always shows a general trend of increase with increasing temperature.

The intershell coupling or charge transfer depends not only on temperature as shown in Figures 4b and 5b but also on the diameter of the carbon nanotube. A recent quantitative study[16] revealed that for an MWCNT the intershell resistance is about 1 Ω·M, and this value is about 1000 to 100 000 times larger than that for a pure graphite. This large intershell resistance results from the lack of structural correlation between different carbon shells in the MWCNT and restrictions imposed by the energy and momentum conservation. As the diameter of the MWCNT increases, we would expect to see an improvement in the intershell coupling, since the discrete k points of the tube now become closer together and momentum conservation may be satisfied more easily than for a smaller tube. Figure 5a shows field-effect characteristics of a larger DWCNT (with a diameter of 4 nm) than that of Figure 4a (3 nm). The source-drain current curves show the similar general trend we found in Figure 4, i.e., the conductance of the DWCNT switches from higher current level in the p-region at large negative V_g to lower current level in the n-region at large positive V_g. However, the gate is seen to be much less effective in Figure 5a than in Figure 4a, leading to a smaller I_{on}/I_{off} ratio and much wider transition region between the high current and low current states. This is because for a larger DWCNT the charge transfer from the outer semiconducting shell into the inner metallic shell is more effective, and as a result, more charges are available to screen the semiconducting shell leading to a much less effective gating. The residual current level at large positive V_g (Figure 5b) shows again the general increasing trend as the temperature increases. The current level is, however, much higher than that shown in Figure 4b for a smaller DWCNT, and the general trend is being perturbed to a much lesser extent by random peaks and dips.

While for a larger DWCNT the increased intershell coupling makes the gate less effective, the effectiveness of the gate may be increased by reducing the thickness of the insulating SiO_2 layer sandwiched between the back gate and the conducting DWCNT. Shown in Figure 6 are field-effect characteristics for a DWCNT having the same diameter as that of Figure 5, i.e., 4 nm, but the thickness of the SiO_2 is being reduced from 200 nm of Figure 5 to 20 nm. The I_{on}/I_{off} ratio is obviously improved, and the current curve in the n-region is no longer featureless as in Figure 5a. The conductance seems to have been switched from good hole-conductance at large negative V_g to poor

electron-conductance at $V_g > -3$ V. Large contact resistance for the electron conductance in the n-region due to the large band bending leads to the appearance of some current peaks in the n-region at low temperature as a result of electron confinement between the contacts and the nanotube. Figure 6b shows both the hole current at the p-region and the electron current at the n-region. The large hole current decreases with increasing temperature, and this may be attributed to the stronger scattering at higher temperature. The electron current, on the other hand, increases with increasing temperature, and we attribute this to the enhanced intershell coupling as previously discussed.

Conclusions

In summary, large-diameter DWCNTs have been used to fabricate FETs, and their electrical characteristics have been investigated. Three distinct types of field-effect characteristics were observed and identified as resulting from S−S, M−M or M−S, and S−M combinations of the two shells of the DWCNT. While a S−S DWCNT shows basically the same field-effect characteristics as that of a semiconducting SWCNT, and a M−M or M−S DWCNT as a metallic SWCNT, the S−M DWCNT shows distinctly new field-effect characteristics. In particular, it was found that the charges transferred into the inner metallic shell may screen the outer semiconducting shell from the gate effect, and the intershell interaction increases with increasing temperature and tube diameter. It is expected that a similar screening effect also plays an important role in the electron transport of MWCNTs, and the effect is particularly important for larger MWCNTs.

Acknowledgment. We thank Prof. H. M. Cheng for kindly providing the DWCNTs used in this study, and M.S. Wang, C.H. Jin, and K. Yao for technique assistance and discussions. This work was supported by the Ministry of Science and Technology (grant 001CB610502), National Science Foundation of China (grants 60271004 and 10434010), the Chinese Ministry of Education (Key Project, grant 10401) and the National Center for Nanoscience and Technology of China.

References and Notes

(1) Tans, S. J.; Verschueren, A. R. M.; Dekker, C. *Nature (London)* **1998**, *393*, 49.
(2) Odom, T. W.; Huang, J. L.; Kim, P.; Lieber, C. M. *Nature (London)* **1998**, *391*, 62.
(3) Frank, S.; Poncharal, P.; Wang, Z. L.; de Heer, W. A. *Science* **1998**, *280*, 1744.
(4) Bockrath, M.; Cobden, D. H.; Lu, J.; Rinzler, A. G.; Smalley, R. E.; Balents, L.; McEuen, P. L. *Nature (London)* **1999**, *397*, 598.
(5) Collins, P. G.; Arnold, M. S.; Avouis, P. *Science* **2001**, *294*, 1317.
(6) Javey, A.; Guo, J.; Wang, Q.; Lundstrom, M.; Dai, H. J. *Nature (London)* **2003**, *424*, 654.
(7) Sanvito, S.; Kwon, Y. K.; Tomanek, D.; Lambert, C. J. *Phy. Rev. Lett.* **2000**, *84*, 1974.
(8) Roche, S.; Triozon, F.; Rubio, A.; Mayou, D. *Phy. Rev. B* **2001**, *64*, 121401(R).
(9) Uryu, S. *Phy. Rev. B* **2004**, *69*, 075402.
(10) Miyamoto, Y.; Satio, S.; Tomanek, D. *Phy. Rev. B* **2001**, *65*, 041402.
(11) Kociak, M.; Suenaga, K.; Hirahara, K.; Saito, Y.; Nakahira, T.; Iijima, S. *Phy. Rev. Lett.* **2002**, *89*, 155501.
(12) Shimada T. *Appl. Phy. Lett.* **2004**, *84*, 2412.
(13) Bachtold, A. *Nature (London)* **1999**, *397*, 673.
(14) Collins, P. G.; Avouris, Ph. *Appl. Phys. A* **2002**, *74*, 329.
(15) Liang, X. L.; Peng, L.-M.; Chen, Q.; Che, R. C.; Xia, Y.; Xue, Z. Q.; Wu, Q. D. *Phy. Rev. B* **2003**, *68*, 073403
(16) Bourlon, B.; Miko, C.; Forro, L.; Glattli, D. C.; Bachtold, A. *Phy. Rev. Lett.* **2004**, *93*, 176806.
(17) Li, L.; Li, F.; Liu, C.; Cheng, H.-M. *Carbon* **2005**, *43*, 623.
(18) Javey, A.; Shim, M.; Dai, H. J. *Appl. Phy. Lett.* **2002**, *80*, 1064.